arXiv:1301.1659v1 [quant-ph] 8 Jan 2013

Strong coupling between single atoms and non-transversal photons

Christian Junge, Danny O'Shea, Jürgen Volz, and Arno Rauschenbeutel
Vienna Center for Quantum Science and Technology
Atominstitut, Vienna University of Technology
Vienna, Austria.

We investigate the interaction between single quantum emitters and non-transversally polarised photons for which the electric field vector amplitude has a significant component in the direction of propagation. Even though this situation seems to be at odds with the description of light as a transverse wave, it regularly occurs when interfacing or manipulating emitters with non-paraxial, guided, or evanescent light. Here, we couple single rubidium atoms to single photons which are confined in an optical microresonator by continuous total internal reflection. We experimentally show that the non-transversal polarisation decisively alters the physics of strong light–matter interaction. This effect has far-reaching and highly advantageous implications, which, e.g., significantly advance the field of cavity quantum electrodynamics with whispering-gallery-mode resonators. In particular, our finding allows us to experimentally realise a paradigmatic quantum system, which is ideally suited for basic studies and technological applications.

The interaction between single atoms and single photons lies at the heart of quantum optics and has been investigated in a number of groundbreaking experiments with high-finesse cavities confining the photons.[1–9] In these cavity quantum electrodynamics (CQED) systems, the strong coupling regime[10, 11] has been reached, meaning that the coherent atom–light coupling dominates over all dissipative processes. This has led to the experimental demonstration of a variety of building blocks for quantum communication and quantum information processing with optical photons.[2, 3, 8, 9] In order to move forward from these proof-of-principle studies, the optical loss of the resonator has to be significantly reduced.[12] Whispering-gallery-mode (WGM) microresonators,[13, 14] which confine light by continuous total internal reflection, and enable near-lossless in- and out-coupling of light via tapered fibre couplers,[15] have been proposed as a solution to this problem. As recently demonstrated in a series of pioneering experiments with toroidal WGM microresonators,[16–19] single atoms can be strongly coupled to WGMs via the evanescent field outside the resonator. This achievement, combined with the high in- and out-coupling efficiency of light,[15] has made it possible, for example, to realise a turnstile as well as a router for photons.[17, 18] Strong coupling between WGMs and solid state quantum emitters has been demonstrated as well.[20, 21] Beyond their importance in strong light–matter coupling, WGM microresonators are highly versatile photonic devices, which have, e.g., enabled label-free detection of single molecules in a bio-compatible environment,[22] on-chip single nanoparticle detection and sizing[23] as well as virus detection,[24] on-chip generation of optical frequency combs,[25] and generation of squeezed and correlated twin-beams as well as single and pair photons.[26, 27] Moreover, WGM microresonators provide a very successful experimental platform in the thriving field of cavity optomechanics.[28, 29]

However, theoretical CQED models thus far predict a fundamental problem in the use of WGM resonators for CQED applications. These models treat WGM microresonators as conventional ring resonators which sustain a pair of degenerate, identically polarised, counterpropagating modes.[16–19, 21, 23, 24, 30–34] Under this assumption, the corresponding standing wave modes are then predicted to exhibit an azimuthal intensity modulation with maximum visibility and phase that can be chosen such that one mode has a node at the position of a given emitter. This uncoupled standing-wave mode would fundamentally limit the performance of WGM microresonators for coupling light and matter. Here, using single rubidium atoms which are strongly coupled to a WGM bottle microresonator,[35–37] we experimentally demonstrate that the non-transversal polarisation of the evanescent field of WGMs inhibits destructive interference, and thus prevents the formation of an uncoupled mode. Our results agree with a model that includes the full vectorial description of the resonator modes and the internal level structure of the atoms. In addition, the non-transversal character of near-field photons leads to a qualitatively new and advantageous physical situation, which fundamentally differs from previous CQED experiments and which opens up a realm of possibilities for technological applications and fundamental studies.

The WGM bottle microresonators employed in our experiment are prolate-shaped cylindrically symmetric silica structures, see Fig 1 **a**, which sustain WGMs with ultra-high quality factor ($Q \gtrsim 10^8$) and small mode volume, compatible with the requirements of CQED in the strong coupling regime.[36, 37] Compared to other types of ultra-high Q WGM microresonators, such as microspheres[38] and microtori,[39] bottle microresonators have the additional advantage of being fully tuneable.[37] Moreover, their mode geometry straightforwardly enables near-lossless simultaneous coupling of two independent tapered fibre couplers.[40]

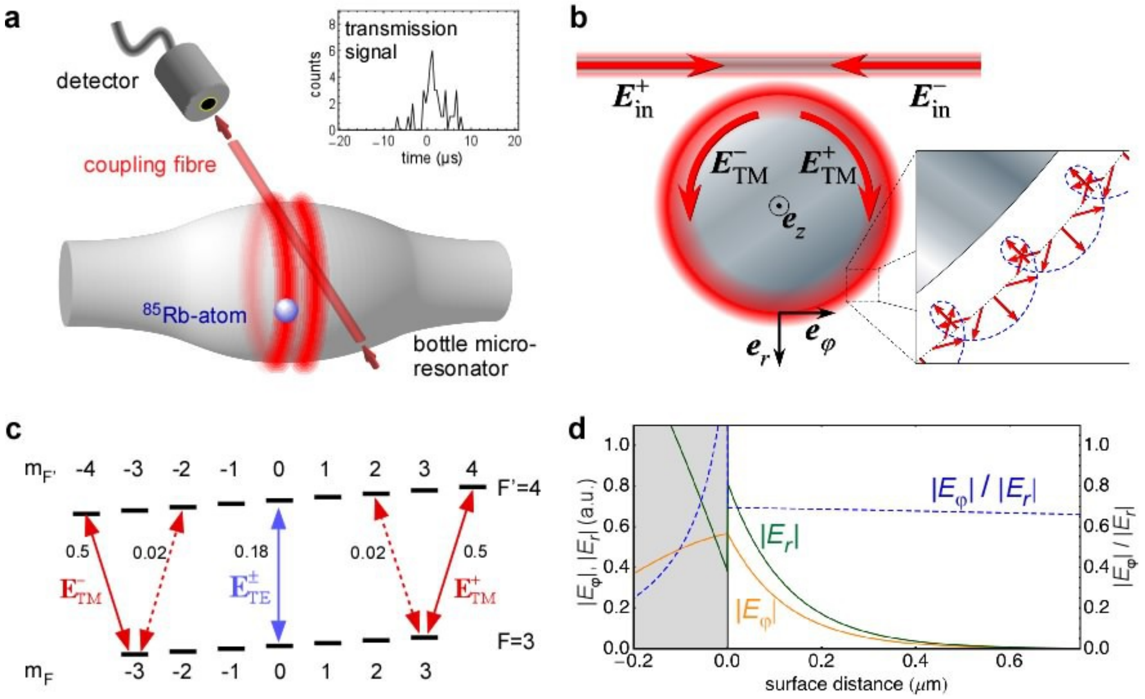

FIG. 1. **Interaction between a single atom and a WGM bottle microresonator.** **a**, Schematic view of our bottle microresonator interfaced with a tapered fibre coupler. Probe light, launched into the coupling fibre, is coupled into the resonator via frustrated total internal reflection and the remaining transmission is detected by a single photon counter. **b**, In the case of TM-modes, the spatial dependence of the electric field vector along the resonator is well described by a cycloid. **c**, Relevant atomic levels and transition strengths for ^{85}Rb. Due to the strong overlap with σ^+ (σ^-) polarisation, TM modes drive $\Delta m_F = +1$ ($\Delta m_F = -1$) transitions, pumping into the Zeeman sublevel with maximum (minimum) m_F, while the π-polarised TE modes drive $\Delta m_F = 0$ transitions. **d**, Longitudinal and transversal electric field components and their ratio as function of the distance to the resonator surface, calculated for the TM modes of our bottle microresonator.

MODELLING THE ATOM–LIGHT INTERACTION

In order to model the interaction of single alkali atoms with bottle microresonator modes (bottle modes), we employ the Jaynes-Cummings Hamiltonian, generalised to a multilevel atom description and the full vectorial treatment of the evanescent electric field of a pair of counter-propagating bottle modes. As in all types of WGM microresonators, bottle modes can be classified according to the orientation of the electric field polarisation, which either lies predominantly in the plane perpendicular to the resonator axis (TM) or predominantly points along this z-axis (TE). TE modes are almost exclusively transversally polarised, i.e., their electric field vector is, to a good approximation, perpendicular to their wave vector at any position of the mode. In qualitative contrast, the TM modes are non-transversally polarised,[41, 42] meaning that the electric field vector of the evanescent field has a non-vanishing component along the wave vector, see Fig. 1 **d**. This longitudinal component oscillates ±90° out of phase with respect to the transversal component. Thus, for a given distance from the resonator surface, the complex-valued amplitude vector of TM modes is

$$\mathbf{E}_{\rm TM}^{\pm} = \mathbf{E}_{\rm trans} \pm i\mathbf{E}_{\rm long} \ . \qquad (1)$$

Here, $\mathbf{E}_{\rm trans} \approx |\mathbf{E}_{\rm trans}|\mathbf{e}_r$ ($\mathbf{E}_{\rm long} = |\mathbf{E}_{\rm long}|\mathbf{e}_\varphi$) is the transversal (longitudinal) amplitude vector with the real-valued radial (azimuthal) unit vector $\mathbf{e}_r$ ($\mathbf{e}_\varphi$). The $+$ ($-$) sign corresponds to the left-handed (right-handed) rotation sense of the mode with respect to the z-axis, which defines our quantisation axis. The situation is much simpler for the TE modes, which have approximately the same amplitude vector for both rotation senses, $\mathbf{E}_{\rm TE}^{+} \approx \mathbf{E}_{\rm TE}^{-} \approx |\mathbf{E}_{\rm TE}^{\pm}|\mathbf{e}_z$, where $\mathbf{e}_z$ is the real-valued axial unit vector.

The sign in Eq. (1) has a decisive influence on the coupling of a degenerate pair of counter-propagating modes to an atom. For the sake of simplicity, let us first assume that $|\mathbf{E}_{\rm trans}| = |\mathbf{E}_{\rm long}|$. In this case, $\mathbf{E}_{\rm TM}^{+}$ and $\mathbf{E}_{\rm TM}^{-}$ describe two modes with mutually orthogonal circular polarisations. However, in contrast to what is usually encountered for freely propagating light fields, the plane of polarisation is parallel to the local wave vector of the mode and the electric field vector describes a cycloid along the circumference of the resonator, see Fig. 1 **b**. Any superposition of such a pair of counter-propagating modes corresponds to a light field with azimuthally symmetric intensity and ellipticity. As a consequence, the atom–light coupling strength is independent of the azimuthal position of the atom or, equivalently, of the relative phase of the superposition. In particular, this rules out the existence of an uncoupled TM mode. This differs fundamentally from what is encountered for standard paraxial Fabry-Pérot and ring-resonators, where this intrinsic connection between polarisation and propagation direction does not occur.

For WGMs with maximal angular momentum, the ratio $|\mathbf{E}_{\mathrm{long}}|/|\mathbf{E}_{\mathrm{trans}}|$ is largely independent of the geometry and the diameter of the WGM resonator and almost exclusively determined by the refractive index of the resonator material (see Methods). For WGM microresonators made of silica, one obtains $|\mathbf{E}_{\mathrm{long}}|/|\mathbf{E}_{\mathrm{trans}}| \approx 0.7$ (see Fig. 1 **d**). Thus, $|\mathbf{E}^{\pm}_{\mathrm{TM}} \cdot \mathbf{e}^{*}_{\sigma^{\pm}}|^2/|\mathbf{E}^{\pm}_{\mathrm{TM}}|^2 > 0.96$, where $\mathbf{e}_{\sigma^{\pm}} = (\mathbf{e}_r \pm i\mathbf{e}_{\varphi})/\sqrt{2}$, meaning that $\mathbf{E}^{\pm}_{\mathrm{TM}}$-modes almost fully overlap with an ideally circularly ($\sigma^{\pm}$) polarised mode. For higher refractive indices, the overlap will be even higher.

Besides preventing the formation of an uncoupled standing wave mode, the near perfect circular polarisation of $\mathbf{E}^{\pm}_{\mathrm{TM}}$ has an additional advantage: Consider the case where the resonator is, e.g., coupled to a single ^{85}Rb atom and light is launched into the coupling fibre in the direction of $\mathbf{E}^{+}_{\mathrm{in}}$ in order to resonantly excite mode $\mathbf{E}^{+}_{\mathrm{TM}}$, see Fig. 1 **b**. The atom then interacts with almost purely circularly polarised (σ^{+}) light and transitions with $\Delta m_F = +1$ are predominantly driven, where m_F is the magnetic quantum number of the atomic hyperfine states. This leads to optical pumping and, when the $\mathbf{E}^{+}_{\mathrm{TM}}$-mode is close to resonance with the atomic transition $5S_{1/2},\ F = 3 \rightarrow 5P_{3/2},\ F' = 4$, the atom is transferred to the outermost Zeeman sublevel with $F = 3, m_F = 3$ after a few scattering events, see Fig. 1 **c**. From there, light in the $\mathbf{E}^{+}_{\mathrm{TM}}$-mode can only excite the $F' = 4, m_{F'} = 4$ state which can only decay back to the $F = 3, m_F = 3$ ground state, thus yielding a closed cycling transition. This situation occurs naturally and is highly advantageous for two reasons: First, the closed cycling transition maximises the coupling strength of the atom to the electromagnetic field. And second, the selection rules for dipole transitions prevent the atom from emitting light into the orthogonally polarised, counter-propagating $\mathbf{E}^{-}_{\mathrm{TM}}$-mode. Despite the simultaneous existence of two degenerate resonator modes, this effectively leads to the ideal case of a two-level atom that only interacts with a single traveling-wave mode. Thus, our theoretical model predicts a spectrum of the coupled atom-resonator system that exhibits the well-known vacuum-Rabi splitting of the resonance frequencies by $\Delta\omega = 2g$, see Fig. 2 **a**, where g is the atom-resonator coupling strength.

A fundamentally different situation is encountered when considering the interaction with a TE-mode. Since both running waves have the same linear polarisation, the atom will interact with both modes and an uncoupled standing wave resonator mode occurs. This leads to qualitatively different physical behaviour compared to TM modes, which is apparent in the predicted spectrum which contains an additional central resonance, that is a signature of the uncoupled standing wave mode, see Fig 2 **b**. We note that this spectrum essentially corresponds to the predictions of the formerly employed theoretical model that neglected the non-transversal polarisation of the resonator modes. This shows that transversely polarised modes are unsuitable for schemes and applications which require the atom to split the transmission spectrum into two dips, such a single photon transistors.[43]

EXPERIMENTAL SPECTRA

In order to verify that the above scenarios adequately describe our experiment, we investigate the physical behaviour of TE and TM modes. Figure 1 **a** shows a schematic of our experimental setup with the bottle microresonator interfaced with a sub-micron diameter coupling fibre.[44–46] We tune the frequency of the bottle microresonator to the atomic $5S_{1/2},\ F = 3 \rightarrow 5P_{3/2},\ F' = 4$ transition of ^{85}Rb (transition wavelength $\lambda = 780$ nm) and critically couple the coupling fibre to the resonator. At this set-point, the in- and out-coupling rate of light matches the intrinsic loss rate of the empty resonator. We set the polarisation of the resonant light in the coupling fibre to match the polarisation of the bottle mode. As a result, the light will be entirely coupled into the bottle microresonator mode and dissipated therein. The remaining transmission through the coupling fibre is typically as low as 1 %, see Fig. 2. We then launch a cloud of laser-cooled ^{85}Rb-atoms towards the resonator. If an atom enters the evanescent field of the resonator-mode, the vacuum Rabi splitting of the resonance frequency of the strongly coupled atom–resonator system results in a significant increase of the coupling fibre transmission, see inset of Fig. 1 **a**. When such an event is registered, a fast optical switch is used to turn off the detection light in realtime and to simultaneously apply a spectroscopy field through the coupling fibre that can be set to any relevant detuning $\Delta_{\mathrm{rs}} = \omega_{\mathrm{r}} - \omega_{\mathrm{s}}$, where $\omega_{\mathrm{r}}/2\pi$ and $\omega_{\mathrm{s}}/2\pi$ are the frequencies of the resonator mode and spectroscopy field, respectively.

Figures 2 **c** and **d** show transmission spectra obtained for the case of probing a TM- and TE-polarised mode, $\mathbf{E}^{+}_{\mathrm{TM}}$ and $\mathbf{E}^{+}_{\mathrm{TE}}$, respectively. A guiding magnetic field $B_z = 4.5$ G along the z-axis lifts the degeneracy of the Zeeman sublevels. The bottle-resonator is set to resonance with the dominant atomic transition ($F = 3,\ m_F = 3 \rightarrow F' = 4,\ m'_F = 4$ for TM and $F = 3,\ m_F = 0 \rightarrow F' = 4,\ m'_F = 0$ for TE). Compared to the case of an atom-resonator system with a well defined coupling constant g (Fig. 2 **a** and **b**), in our experiment the coupling strength of the atoms varies, both during the transit and from shot to shot. We account for this by fitting an averaged spectrum to the transmission data, where the only free fit parameters are the mean value of the coupling strength $\bar{g}$ and its standard deviation σ_g (see Methods). Perfect agreement is found between the experimental data and the theoreti-

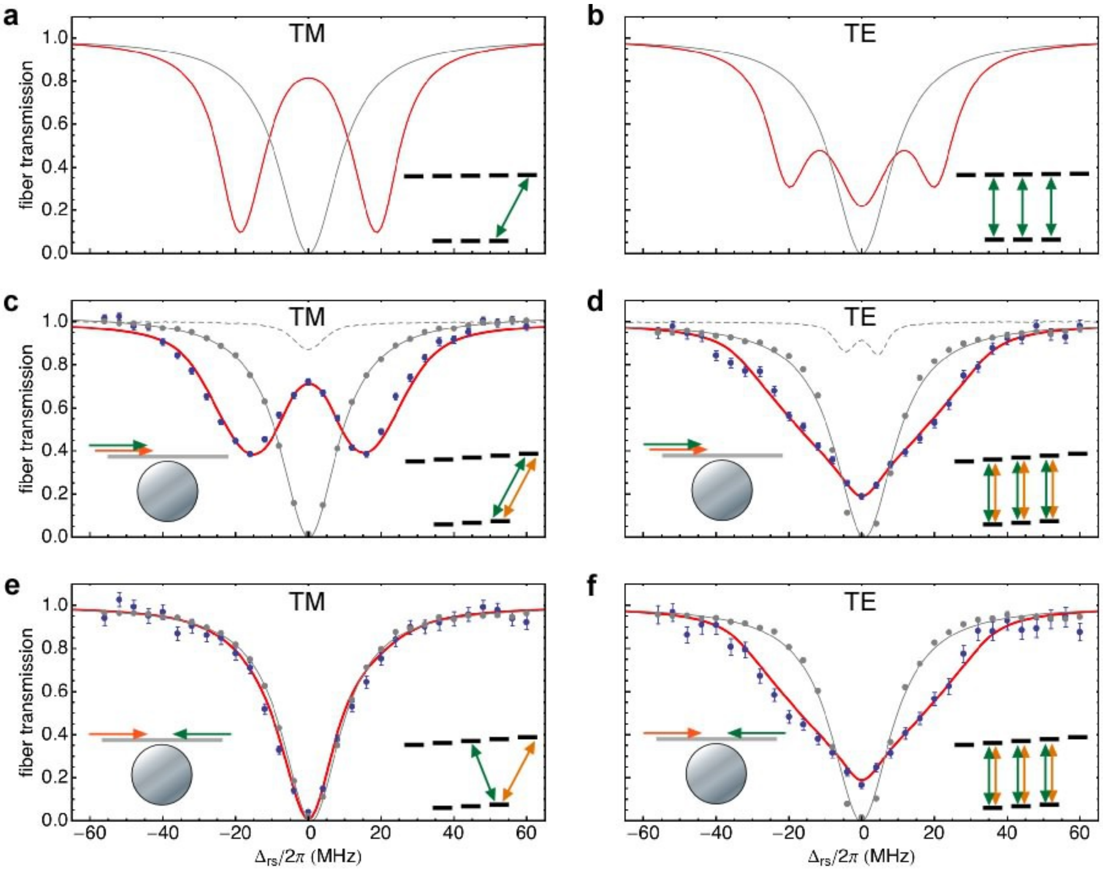

FIG. 2. **Vacuum Rabi-splitting for TM and TE modes.** **a** and **b**, Calculated coupling fibre transmission for a TM and a TE mode, respectively, coupled to a single atom with a fixed coupling strength of $g/2\pi = 20$ MHz and zero atom–resonator detuning (red line). The transmission for an empty resonator is shown by the grey line. **c** and **d**, Measured fibre transmission for our TM and TE mode, respectively, (blue circles: experimental data; error bars indicate the 1σ statistical error) with a guiding field of $B_z = 4.5$ G. The resonator is resonant with the transition $F = 3,\ m_F = 3 \rightarrow F' = 4,\ m'_F = 4$ and $F = 3,\ m_F = 0 \rightarrow F' = 4,\ m'_F = 0$, respectively. The red solid line is a theoretical fit yielding an average coupling strength of $\bar{g}/2\pi = 17$ MHz with a standard deviation of $\sigma_g/2\pi = 6$ MHz and $\sigma_g/2\pi = 9$ MHz, respectively (see Methods). The grey data shows the transmission of the empty cavity with a Lorentzian fit yielding a HWHM of $\kappa/2\pi = 10$ MHz. The dashed lines are the measured empty resonator transmission spectra of the respective mode in the undercoupled regime. **e** and **f**, Vacuum Rabi spectrum measured under same conditions as in **c** and **d** but applying the spectroscopy laser from the opposite direction as the detection laser. To avoid optical pumping by the spectroscopy laser, the spectrum is only measured for the first 100 ns. The theory curves are calculated using the same parameters $\bar{g}$ and σ_g as in **c** and **d**, respectively. The insets show the direction of the detection (orange) and the spectroscopy light (green) and a simplified atomic level scheme indicating the driven transitions.

cally predicted spectra. As expected, for the $\mathbf{E}^+_{\mathrm{TM}}$-mode, the spectrum clearly features two transmission dips while the spectrum for the $\mathbf{E}^+_{\mathrm{TE}}$-mode is dominated by a central dip.

We now launch the detection light along $\mathbf{E}^+_{\mathrm{in}}$ and the spectroscopy light along the opposite direction $\mathbf{E}^-_{\mathrm{in}}$. For the TE polarised mode, we expect the same transmission spectrum as before. However, the situation is different for the TM modes, where we populate the $\mathbf{E}^+_{\mathrm{TM}}$-mode during detection and the atom is pumped into the $m_F = 3$ state. The spectroscopy is then carried out on the $\mathbf{E}^-_{\mathrm{TM}}$-mode, which initially drives the $F = 3,\ m_F = 3 \rightarrow F' = 4,\ m'_F = 2$ transition, see Fig. 1 **c**. However, this transition is strongly suppressed by two effects. First, its strength is more than one order of magnitude smaller than for the closed cycling transition, and second, the strong interaction of the atom with the empty $\mathbf{E}^+_{\mathrm{TM}}$-mode on the $F = 3,\ m_F = 1 \rightarrow F' = 4,\ m'_F = 2$ transition leads to a vacuum Rabi splitting of the excited state. As a result, the transmission spectrum recorded with detection and spectroscopy light launched from opposite sides should initially closely resemble that of an empty resonator. Figure 2 **e** (**f**) shows the transmission spectra of the TM (TE) mode recorded for this case. The interaction time of the spectroscopy field with the coupled atom–resonator system was limited to the first 100 ns after the initial relaxation of the resonator field in order to prevent optical depumping of the initial atomic state. The transmission spectrum predicted by our model in Figs. 2 **e** and **f** (solid lines with the same values of g

and σ as in Figs. 2 **c** and **d**) shows excellent agreement between experiment and theory.

RESONATOR-INDUCED OPTICAL PUMPING

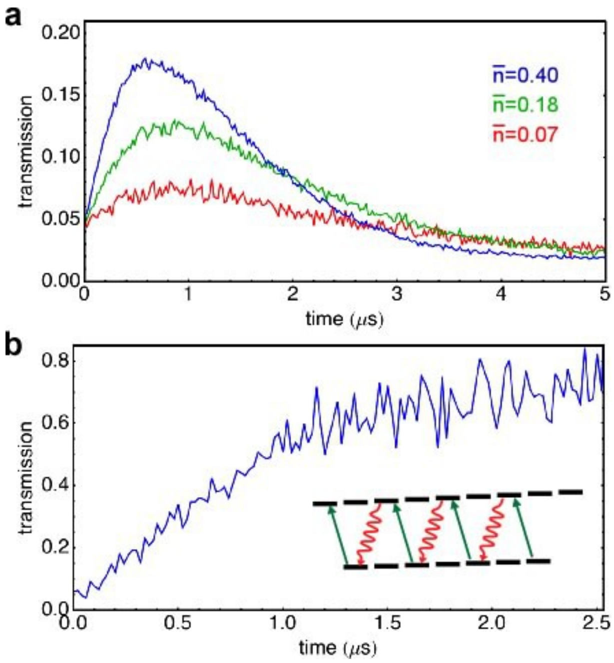

FIG. 3. **Optical pumping in TM modes.** **a**, On-resonance coupling fibre transmission for the TM mode as function of time, when the spectroscopy light field is applied from the opposite direction as the probe light. A guiding field of $B_z = 4.5$ G is applied and the resonator is set to resonance with the transition $F = 3,\ m_F = 3 \rightarrow F' = 4,\ m'_F = 4$. The curves correspond to three different probe powers leading to a mean photon number of $\bar{n} = 0.07$ (red), 0.18 (green) and 0.4 (blue) in the resonator mode in the absence of an atom. Over time, the probe light pumps the atom into $F = 3,\ m_F = -3$ resulting in an increasing coupling strength between atom and resonator. The initial slopes of the transmission are 0.06 μs^{-1}, 0.18 μs^{-1} and 0.37 μs^{-1}, respectively, and increase linearly with power. The drop in transmission for larger times t is caused by atom loss. **b**, Same as the blue data in **a**, but conditioned to a second atom detection at $t = 2.5$ μs, in order to discard runs where the atom was lost. The transmission increases from its initial value of 5% to a value of more than 60% in good agreement with the on-resonance transmission expected in the steady state.

If the spectroscopy light is applied from the opposite side as the detection light for longer time intervals, the atom will eventually scatter photons from the $\mathbf{E}^{-}_{\mathrm{TM}}$-mode into the initially empty $\mathbf{E}^{+}_{\mathrm{TM}}$-mode and change its Zeeman sublevel by $\Delta m_F = -2$ in this process. After three such scattering events, it will therefore end up being optically pumped into the $m_F = -3$ state, see inset Fig. 3 **b**. This means that the on-resonance transmission of the spectroscopy light is expected to increase while we gradually recover the case of a two-level atom interacting with a single resonator mode. Figure 3 **a** shows this on-resonance transmission as a function of interaction time for three different intracavity photon numbers. We initially observe a linear increase of the transmission with a slope that is proportional to the photon flux. For even longer interaction times, the transmission drops to zero because the atom ends up leaving the resonator mode. If we select only those events in which the atom is still present in the resonator mode after 2.5 μs, we obtain the transmission time trace presented in Fig. 3 **b**. In this case, the transmission reaches more than 60%, which corresponds to the transmission expected in the steady state case for our system and which indicates that the atom has been pumped to the $m_F = -3$ state during the measurement.

In order to further verify that the above-described scenario occurs in our experiment, we have recorded transmission spectra for the TM polarised mode with different values of B_z. For the spectra presented in Figs. 4 **a** and **b**, the resonator was resonant with the atomic transition frequency in zero magnetic field, and B_z was set to +4.5 G and −3 G, respectively. The asymmetry in the shape of the dips in the spectra is well reproduced by the theory and stems from the magnetic field-induced detuning of the closed cycling transition with respect to the resonator. The sign of this shift depends on the sign of B_z. Then, we launched detection and spectroscopy light fields into the coupling fibre from the opposite side, meaning that it will be exclusively coupled into the $\mathbf{E}^{-}_{\mathrm{TM}}$-mode. Thus, we expect the atom to be optically pumped into the $m_F = -3$ state, thereby changing the sign of the Zeeman shift of the atomic transition frequency. Figures 4 **c** and **d** show that the asymmetry is, as expected, inverted in this case. This provides an additional confirmation that the atoms are indeed optically pumped to the extreme Zeeman states during their interaction with the resonator mode.

CONCLUSIONS

Summarising, we experimentally demonstrated that the longitudinal component of the electric field in whispering-gallery-modes inhibits destructive interference between counter-propagating photons and thereby qualitatively changes the coupling of light and matter. This effect is universal in the sense that it stems from the physics of total internal reflection. For this reason, it is largely independent of the size and geometry of the resonator and will also occur for other resonator materials. In the context of the CQED experiment presented here, it leads to an unexpectedly clean situation, close to the ideal case of a two-level atom that strongly interacts with one single mode of the electromagnetic field. In combination with the demonstrated low optical losses of whispering-gallery-mode microresonators, this constitutes ideal conditions for the realisation of photonic

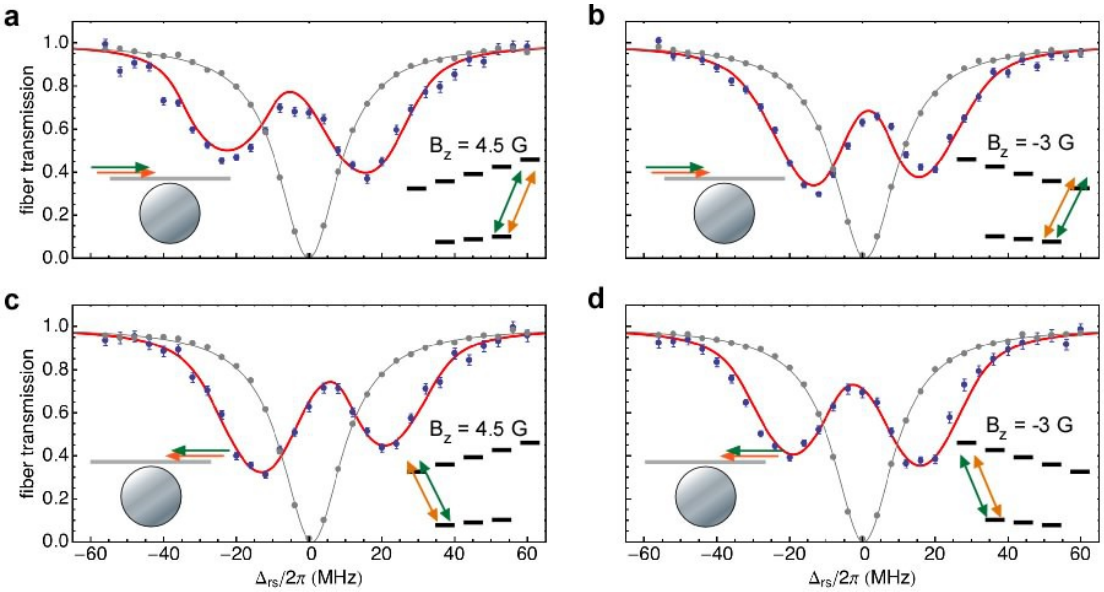

FIG. 4. **Vacuum Rabi splitting for different magnetic fields.** **a** and **b**, Measured coupling fibre transmission (blue circles: experimental data; error bars indicate the 1σ statistical error) for the TM-mode with a guiding field of $B_z = 4.5$ G and $B_z = -3$ G, respectively, and zero resonator–atom detuning for the $F = 3,\ m_F = 0 \rightarrow F' = 4,\ m'_F = 0$ transition. The red solid lines are theoretical model fits with average coupling strengths of $\bar{g}/2\pi = 19$ MHz and $\bar{g}/2\pi = 16$ MHz, respectively. **c** and **d**, Same as **a** and **b**, but with detection and spectroscopy light applied from the opposite direction. In this case, the theoretical model fits yields an average coupling constant of $\bar{g}/2\pi = 17$ MHz and $\bar{g}/2\pi = 18$ MHz, respectively. The asymmetry results from the magnetic field induced detuning of the closed cycling transition and is well reproduced by the theory. The standard deviation of the coupling strength for all fits is $\sigma_g/2\pi = 7$ MHz.

quantum devices in optical fibre-based networks. Such an architecture would strongly profit from a design where quantum emitters are permanently coupled to the resonator modes. This could be realised, for example, with solid-state-based systems in the resonator mode[20, 21] or by trapping laser-cooled atoms in the evanescent field of auxiliary whispering-gallery-modes[47] or of a nearby optical nanofibre.[48]

METHODS

A. Atom source

In our experiment, we prepare a cloud of about 5×10^7 laser-cooled ^{85}Rb atoms in a magneto-optical trap and launch it upwards by means of a moving molasses[45]. The bottle microresonator is approximately located at the turning point of the ballistic trajectory of the atomic cloud. The atom cloud overlaps with the bottle microresonator for about 50 ms. During this time interval, a small number of individual atoms will enter into the evanescent field of the WGM at random arrival times. The temperature of the atom cloud is about 5 μK, which yields a thermal velocity on the order of a few cm/s. In conjunction with the decay length of the evanescent field of the bottle microresonator of about 118 nm, this gives rise to expected average interaction times of a few microseconds, in good agreement with the observed transits. We checked that the number of atom transits depends strictly linearly on the density of the atomic cloud. This allows us to conclude that the observed coupling events are indeed transits of individual single atoms through the resonator field.

B. Real-time atom detection and spectroscopy

The arrival time of atoms at the bottle microresonator is inherently random. Thus, an active detection scheme is applied, that can detect the presence of an atom in the cavity mode in real time. For this purpose, we set the coupling fibre to critical coupling and apply a detection light field with a flux of 1.2×10^7 photons/s, corresponding to a mean photon number of 0.18 in the resonator mode. We continuously monitor the coupling fibre transmission using single photon counting avalanche photodiodes. A trigger and control system, based on a fast field programmable gate array, registers the photon detection events. As soon as the number of detected photons within a predetermined time interval $\Delta t_1 = 1.2$ μs exceeds a user-defined threshold value $\eta_1 = 6$ (TM) or $\eta_1 = 4$ (TE), respectively, the system generates a trigger. This in turn operates a fast optical switch, that turns off the detection light and switches on a spectroscopy field that can be set to any relevant detuning in advance. The spectroscopy light is applied for a predetermined time interval ranging from 100 ns to a few microseconds. We then switch back to the probe light in order to check if the atom is still present, using a detection time interval of $\Delta t_2 = 1$ μs and a threshold value of $\eta_2 = 2$ photons. Events where the atom was lost are discarded. For the spectra presented in this work, we typically average the transmission over about 1000 atom transits for each detuning of the spectroscopy light.

C. Bottle resonator modes

In contrast to other WGM resonators, bottle-resonators sustain a large quantity of higher order axial modes,[37] which strongly differ by the intrinsic scattering rate between the two counterpropagating modes. We estimate the axial mode number by imaging the scattered light from the empty resonator, which allows us to roughly infer the spatial extension of the cavity field. In order to achieve a high coupling strength in our experiment, we select high-Q modes with minimal axial mode number, which feature a low intrinsic scattering rate at the same time. We infer the latter from the intrinsic splitting of the empty resonator transmission spectrum in the undercoupled regime, see Fig 2 **c** and **d**. For the modes investigated here, we estimate an axial mode number of $q \lesssim 2$ ($q \lesssim 4$) and an intrinsic mode splitting of smaller than 1 MHz (8 MHz) for the TM (TE) mode.

D. Polarisation of evanescent fields

When light undergoes total internal reflection at a dielectric interface with refractive indices $n_1 > n_2$, the amplitude of the two evanescent electric field components of TM waves is given by:[41, 42]

$$E_r = E_0 \frac{2\cos\theta\sin\theta}{(n^4\cos^2\theta + \sin^2\theta - n^2)^{1/2}} \tag{2}$$

$$E_\varphi = iE_0 \frac{2\cos\theta(\sin^2\theta - n^2)^{1/2}}{(n^4\cos^2\theta + \sin^2\theta - n^2)^{1/2}}, \tag{3}$$

where θ is angle of incidence and $n = n_2/n_1 < 1$ is the ratio of the two refractive indices. The optical modes of WGM we are interested in propagate close to the surface, which results in a large angle of incidence $\theta \approx \pi/2$. The ratio of the two electric field components at the boundary then is

$$\left|\frac{E_\varphi}{E_r}\right| = \sqrt{1-n^2}, \tag{4}$$

and is approximately constant in the evanescent field.

E. Modelling the transmission spectra

For the description of CQED in our bottle microresonator system, we start with the Janyes-Cummings Hamiltonian describing the interaction of a two-level atom with two optical modes, as used in references[16, 21, 30, 31, 33], for example. We extend this model to include the full Zeeman substructure of the atom and the polarisation of the optical modes. Intrinsic scattering between the two counter-propagating bottle mode is experimentally found to be smaller than atom-resonator coupling rate g as well as the decay rate of the resonator field and was thus neglected in the modelling the presented spectra. Since g depends on the distance between the atom and the resonator surface in our experiment, it changes during the atom transits and from shot to shot. We account for this distribution of coupling strengths by fitting an averaged spectrum to the transmission data. For the averaging, we assume the coupling strengths to be normally distributed within an interval ranging from $g/2\pi = 7.5$ MHz to 30 MHz. The latter value corresponds to the expected maximum coupling strength at an atom–resonator distance of 50 nm. For smaller distances, the atom–surface interaction leads to significant shifts of the atomic transition frequencies which effectively inhibit the atom–resonator coupling.

ACKNOWLEDGEMENTS

We gratefully acknowledge financial support by the European Science Foundation and the Volkswagen Foundation. J.V. acknowledges support by the European Commission (Marie Curie IEF Grant 300392). C.J. acknowledges support by the German National Academic Foundation.

---

[1] K. M. Birnbaum, A. Boca, R. Miller, A. D. Boozer, T. E. Northup, and H. J. Kimble, Nature **436**, 87 (2005).

[2] A. D. Boozer, A. Boca, R. Miller, T. E. Northup, and H. J. Kimble, Phys. Rev. Lett. **98**, 193601 (2007).

[3] T. Wilk, S. Webster, A. Kuhn, and G. Rempe, Science **317**, 488 (2007).

[4] M. L. Terraciano, R. Olson Knell, D. G. Norris, J. Jing, A. Fernandez, and L. A. Orozco, Nat. Phys. **5**, 480 (2009).

[5] T. Kampschulte, W. Alt, S. Brakhane, M. Eckstein, R. Reimann, A. Widera, and D. Meschede, Phys. Rev. Lett. **105**, 153603 (2010).

[6] J. Volz, R. Gehr, G. Dubois, J. Esteve, and J. Reichel, Nature **475**, 210 (2011).

[7] C. Sayrin, I. Dotsenko, X. Zhou, B. Peaudecerf, T. Rybarczyk, S. Gleyzes, P. Rouchon, M. Mirrahimi, H. Amini, M. Brune, J.-M. Raimond, and S. Haroche, Nature **477**, 73 (2011).

[8] H. P. Specht, C. Nolleke, A. Reiserer, M. Uphoff, E. Figueroa, S. Ritter, and G. Rempe, Nature **473**, 190 (2011).

[9] S. Ritter, C. Nolleke, C. Hahn, A. Reiserer, A. Neuzner, M. Uphoff, M. Mucke, E. Figueroa, J. Bochmann, and G. Rempe, Nature **484**, 195 (2012).

[10] P. R. Berman, ed., *Cavity Quantum Electrodynamics* (Academic Press, 1994).

[11] K. J. Vahala, Nature **424**, 839 (2003).

[12] H. J. Kimble, Nature **453**, 1023 (2008).

[13] A. Matsko and V. Ilchenko, Selected Topics in Quantum Electronics, IEEE Journal of **12**, 3 (2006).

[14] V. Ilchenko and A. Matsko, Selected Topics in Quantum Electronics, IEEE Journal of **12**, 15 (2006).

[15] S. M. Spillane, T. J. Kippenberg, O. J. Painter, and K. J. Vahala, Phys. Rev. Lett. **91**, 043902 (2003).

[16] T. Aoki, B. Dayan, E. Wilcut, W. P. Bowen, A. S. Parkins, T. J. Kippenberg, K. J. Vahala, and H. J. Kimble, Nature **443**, 671 (2006).

[17] B. Dayan, A. Parkins, T. Aoki, E. Ostby, K. Vahala, and H. Kimble, Science **319**, 1062 (2008).

[18] T. Aoki, A. S. Parkins, D. J. Alton, C. A. Regal, B. Dayan, E. Ostby, K. J. Vahala, and H. J. Kimble, Phys. Rev. Lett. **102**, 083601 (2009).

[19] D. J. Alton, N. P. Stern, T. Aoki, H. Lee, E. Ostby, K. J. Vahala, and H. J. Kimble, Nat. Phys. **7**, 159 (2010).

[20] Y. Park, A. Cook, and H. Wang, Nano Lett. **6**, 2075 (2006).

[21] K. Srinivasan and O. Painter, Nature **450**, 862 (2007).

[22] A. M. Armani, R. P. Kulkarni, S. E. Fraser, R. C. Flagan, and K. J. Vahala, Science **317**, 783 (2007).

[23] J. Zhu, S. K. Ozdemir, Y.-F. Xiao, L. Li, L. He, D.-R. Chen, and L. Yang, Nat. Photon. **4**, 46 (2010).

[24] L. He, S. K. Ozdemir, J. Zhu, W. Kim, and L. Yang, Nat. Nano. **6**, 428 (2011).

[25] P. Del'Haye, A. Schliesser, O. Arcizet, T. Wilken, R. Holzwarth, and T. J. Kippenberg, Nature **450**, 1214 (2007).

[26] J. U. Fürst, D. V. Strekalov, D. Elser, A. Aiello, U. L. Andersen, C. Marquardt, and G. Leuchs, Phys. Rev. Lett. **106**, 113901 (2011).

[27] M. Förtsch, J. Fürst, C. Wittmann, D. Strekalov, A. Aiello, M. V. Chekhova, C. Silberhorn, G. Leuchs, and C. Marquardt, arXiv:1204.3056 (2012).

[28] T. J. Kippenberg and K. J. Vahala, Science **321**, 1172 (2008).

[29] G. Bahl, M. Tomes, F. Marquardt, and T. Carmon, Nat. Phys. **8**, 203 (2012).

[30] P. Domokos, M. Gangl, and H. Ritsch, Opt. Commun. **185**, 115 (2000).

[31] M. Rosenblit, P. Horak, S. Helsby, and R. Folman, Phys. Rev. A **70**, 053808 (2004).

[32] K. Srinivasan and O. Painter, Phys. Rev. A **75**, 023814 (2007).

[33] J. T. Shen and S. Fan, Phys. Rev. A **79**, 23838 (2009).

[34] N. P. Stern, D. J. Alton, and H. J. Kimble, New J. Phys. **13**, 085004 (2011).

[35] M. Sumetsky, Opt. Lett. **29**, 8 (2004).

[36] Y. Louyer, D. Meschede, and A. Rauschenbeutel, Phys. Rev. A **72**, 031801 (2005).

[37] M. Pöllinger, D. O'Shea, F. Warken, and A. Rauschenbeutel, Phys. Rev. Lett. **103**, 053901 (2009).

[38] V. Braginsky, M. Gorodetsky, and V. Ilchenko, Physics Letters A **137**, 393 (1989).

[39] D. K. Armani, T. J. Kippenberg, S. M. Spillane, and K. J. Vahala, Nature **421**, 925 (2003).

[40] M. Pöllinger and A. Rauschenbeutel, Opt. Express **18**, 17764 (2010).

[41] D. Axelrod, T. Burghardt, and N. Thompson, Annu. Rev. Biophys. Bio. **13**, 247 (1984).

[42] T. Kawalec, L. Józefowski, J. Fiutowski, M. Kasprowicz, and T. Dohnalik, Optics Communications **274**, 341 (2007).

[43] P. Bermel, A. Rodriguez, S. G. Johnson, J. D. Joannopoulos, and M. Soljačić, Phys. Rev. A **74**, 043818 (2006).

[44] D. O'Shea, A. Rettenmaier, and A. Rauschenbeutel, Appl. Phys. B **99**, 623 (2010).

[45] D. O'Shea, C. Junge, M. Pöllinger, A. Vogler, and A. Rauschenbeutel, Appl. Phys. B **105**, 129 (2011).

[46] C. Junge, S. Nickel, D. O'Shea, and A. Rauschenbeutel, Opt. Lett. **36**, 3488 (2011).

[47] D. Vernooy and H. Kimble, Phys. Rev. A **55**, 1239 (1997).

[48] E. Vetsch, D. Reitz, G. Sagué, R. Schmidt, S. Dawkins, and A. Rauschenbeutel, Phys. Rev. Lett. **104**, 203603 (2010).